

Enhanced Photoelectrochemical Activity in All-Oxide Heterojunction Devices Based on Correlated “Metallic” Oxides

Brent A. Apgar, Sungki Lee, Lauren E. Schroeder, and Lane W. Martin*

Solar photocatalysis, or the direct conversion of visible light energy to chemical energy, is being considered for a range of applications including the generation of chemical fuels, environmental remediation of organic chemical pollution, and others.^[1,2] At its most basic, a photocatalytic cell provides a photo-anode and -cathode for oxidation and reduction reactions, respectively. The requirements for high-performance solar photocatalytic material systems are clear: broad absorption of the solar spectrum, efficient transfer of charge to the solid-liquid interface, and chemical stability under illumination in solution.

Traditional semiconductors such as silicon and GaAs have band gap energies that permit them to absorb a large portion of the solar spectrum; however, these materials are not stable in solution.^[3,4] Wide band gap oxide materials, by comparison, often possess excellent chemical stability in solution but their large band gap energies make them poor visible light absorbers. A natural approach, then, is to combine these two materials into single systems such as core-shell nanoparticles and heterojunction films.^[5,6] In such semiconductor/oxide heterostructures, however, the transfer of photoexcited carriers to the oxide surface may be limited due to the electronic mismatch of the materials^[7] and oxidation of the light-absorbing semiconductor which can detrimentally affect charge transport.^[8]

Here we investigate a new variation of this methodology whereby we integrate chemically compatible correlated “metallic” oxides with the model n-type, wide band gap oxide semiconductor TiO₂ to produce high-performance photocatalytic heterojunctions. These composite structures operate on the principle of hot carrier injection from the “metallic” oxide into the TiO₂. These effects are made possible by harnessing the diverse range of correlated electron physics of common “metallic” oxide materials including n-type LaNiO₃, SrRuO₃, and SrVO₃ and p-type La_{0.5}Sr_{0.5}CoO₃ and La_{0.7}Sr_{0.3}MnO₃. These materials have been extensively explored (individually) for their novel electronic transport, magnetic properties, and other

exotic physical phenomena,^[9–15] and are widely utilized as epitaxial bottom electrodes in ferroic heterostructures.^[16] Despite this previous work, the potential of these systems for energy applications has only begun to be explored. In the end, the unique electronic structure and density of states (DOS) of these correlated “metallic” oxides gives rise to dramatically different optical properties as compared to traditional metals including strong visible light absorption that significantly enhances photocatalytic activity and enables the study of n-n Schottky, n-n ohmic, and p-n Schottky heterojunctions with TiO₂. We compare and contrast the relative merits of these heterojunction types and explore enhancements in activity made possible by using these systems.

50 nm thick epitaxial thin films of the correlated “metallic” oxides SrRuO₃, LaNiO₃, SrVO₃, La_{0.7}Sr_{0.3}MnO₃, and La_{0.5}Sr_{0.5}CoO₃ were grown on SrTiO₃ (001) and LaAlO₃ (001) substrates via pulsed-laser deposition (see Supporting Information). In all cases, high-quality single-phase films of the “metallic” oxides grow (00l)-oriented, in a cube-on-cube fashion (Figure 1). The films exhibit metal-like conductivity consistent with prior reports (see Supporting Information, Figure S1a).^[9,12,17–19] While often referred to as “metals” due to the presence of decreasing resistivity with temperature, these materials are not “metals” in the traditional sense. Unlike classical metals which owe their electrical transport properties to free electrons, the electrical transport properties observed in these correlated “metallic” oxides come from a combination of complex electronic structures, electron correlations, defect-induced self-doping, cation alloying, and other effects. Transport measurements of these materials reveal high carrier concentrations (>10²¹–10²² cm⁻³) and low majority carrier mobility (0.1 – 10 cm² V⁻¹ s⁻¹) (Figure S1b).

Although the electronic transport,^[20–22] magnetic and electronic structure,^[23–26] and other aspects of these materials have been widely studied, the optical properties have not. Overall, the ability of a material to absorb light is a complex function of the electron energy-momentum (*E-k*) band structure and the electronic DOS. Due to the interest in these materials in the condensed matter physics community, the electronic structure of these “metallic” oxides has been studied extensively^[27–31] and quick analysis of this data suggests that these materials could be promising candidates for strong light absorption. In this spirit, we have explored a range of correlated “metallic” oxides using spectroscopic ellipsometry to extract the reflectance (*R*) and absorption coefficient (*α*) from the optical constants *n* and *k* (Figure S2). *R* and *α* for the n-type materials SrRuO₃ (Figure 2a), LaNiO₃ (Figure 2b), and SrVO₃ (Figure 2c) and the

B. A. Apgar, S. Lee, L. E. Schroeder, Prof. L. W. Martin
Department of Materials Science and Engineering
and Materials Research Laboratory
University of Illinois
Urbana-Champaign, Urbana, IL, 61801, USA
E-mail: lwmartin@illinois.edu

B. A. Apgar, S. Lee, L. E. Schroeder, Prof. L. W. Martin
International Institute for Carbon Neutral Energy Research
744 Motoooka, Nishi-ku, Fukuoka, 819-0395, Japan



DOI: 10.1002/adma.201303144

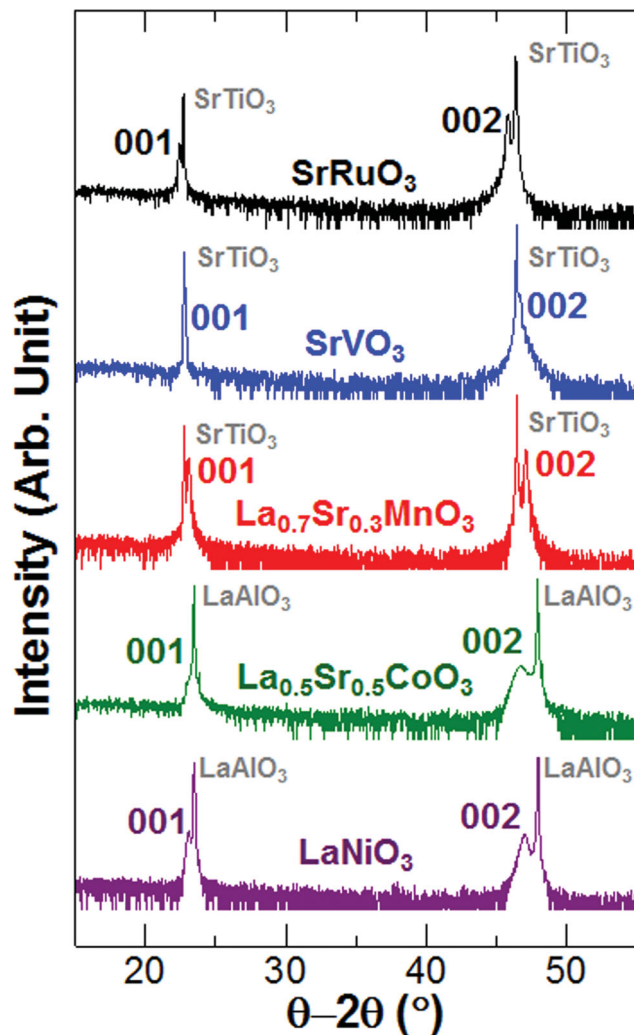


Figure 1. θ - 2θ x-ray diffraction scan of 50 nm epitaxial thin films of SrRuO₃, SrVO₃, and La_{0.7}Sr_{0.3}MnO₃ on SrTiO₃ (001) and of La_{0.5}Sr_{0.5}CoO₃ and LaNiO₃ on LaAlO₃ (001) (top to bottom).

p-type materials La_{0.7}Sr_{0.3}MnO₃ (Figure 2d) and La_{0.5}Sr_{0.5}CoO₃ (Figure 2e) are provided.

Effective light absorbing materials should possess low reflectance as is observed for all the “metallic” oxides studied herein. Additionally, using the measured reflectance values we can calculate the total reflectance of the AM1.5G spectrum for La_{0.5}Sr_{0.5}CoO₃, LaNiO₃, SrRuO₃, La_{0.7}Sr_{0.3}MnO₃, and SrVO₃ to be 33%, 26%, 23%, 20%, and 17%, respectively. These values of total reflectance are significantly lower than those of traditional metals^[32] (generally >90%) and comparable to traditional semiconductors such as In_{0.10}Ga_{0.90}As (37%).^[33,34] All the films are visibly opaque and the optical properties are independent of the underlying substrate. SrRuO₃, SrVO₃, and La_{0.7}Sr_{0.3}MnO₃ (Figure 2a, c, and d, respectively) show similar trends in both reflectance and absorption coefficient – relatively flat, low reflectance at all wavelengths and a strong up-turn in the absorption coefficient near 3.1 eV or 400 nm. LaNiO₃ and La_{0.5}Sr_{0.5}CoO₃, on the other hand (Figure 2b and e), show reflectance that

steadily increases with increasing wavelength and relatively invariant absorption coefficients across the entire range of wavelengths. The implications of these observations for energy applications are illustrated by the fact that a 50 nm thick film of La_{0.5}Sr_{0.5}CoO₃, LaNiO₃, SrRuO₃, La_{0.7}Sr_{0.3}MnO₃, and SrVO₃ will absorb 53%, 50%, 44%, 41%, and 33%, respectively, of the AM1.5G spectrum from 280 to 1300 nm which is comparable to the 50% absorbed by 50 nm of In_{0.10}Ga_{0.90}As^[33,34] and much greater than the 0.62% absorbed by 50 nm of TiO₂^[35] (details of this calculation are provided in the Supporting Information).

The absorption coefficient and reflectance may be understood in terms of the differences in electronic structure of the individual materials. All the systems studied herein are known to possess overlapping electronic bands of different types within the range of excitation energies provided by the AM1.5G spectrum (± 4.5 eV of the Fermi energy, E_F). This continuous DOS provides for a large range of optical transitions and the observed non-zero absorption across the entire wavelength range studied. The fine structure of the absorption can be understood as a result of slight differences in the DOS. The following discussion provides schematic illustrations of the DOS of these “metallic” oxides and is meant to provide a qualitative picture of the possible mechanisms for light absorption based on prior studies of the electronic structure of these materials.

Beginning first with SrRuO₃, there is a high electronic DOS at the E_F associated with a quasiparticle band and occupied and unoccupied portions of the split Ru t_{2g} bands as a result of electron correlations (Figure 2f).^[36] As a result, there is essentially a continuous DOS above E_F which allows for optical inter- and intra-band transitions between states and corresponding continuous light absorption across the solar spectrum with the rise in absorption at 2.5 eV originating from electron transitions from the occupied O $2p$ band to the unoccupied t_{2g} band.^[37] Likewise, in LaNiO₃, where electron correlations are stronger, the Ni t_{2g} and e_g bands are also split, but there is no quasiparticle band and the principal transitions from visible light are almost entirely from the occupied, upper t_{2g} and O $2p$ bands (just below the E_F) to the unoccupied upper e_g band^[38] leading to a relatively invariant absorption coefficient (Figure 2g). In SrVO₃, however, electron correlations result in a splitting of the V t_{2g} and e_g bands, with the E_F located within the overlap of the upper t_{2g} and O $2p$ bands (Figure 2h). Unlike in SrRuO₃ and LaNiO₃, however, there is an energy gap just below E_F which results in the rise in absorption coefficient at around 3 eV when electrons are excited from the occupied O $2p$ band to E_F .^[28]

Similar effects exist in La_{0.7}Sr_{0.3}MnO₃ and La_{0.5}Sr_{0.5}CoO₃ (although the DOS sub-band structure for both materials is more complex than for the n-type oxides as a result of magnetic and spin-lattice effects)^[39–42] where the DOS below the E_F is primarily of O $2p$ character and the above- E_F DOS primarily has Mn or Co $3d$ character. The overlap of these two bands occurs around E_F and yields a continuous DOS. In the case of La_{0.7}Sr_{0.3}MnO₃, the DOS at E_F is relatively low as compared to the DOS located within a few eV on either side of E_F resulting in a small, but continuous absorption of light and a strong turn-on of absorption at around 3.2 eV (Figure 2i). In La_{0.5}Sr_{0.5}CoO₃ the DOS at the E_F is considerably higher compared to the DOS within a few eV on either side of E_F giving rise to a high, yet relatively invariant absorption coefficient (Figure 2j).

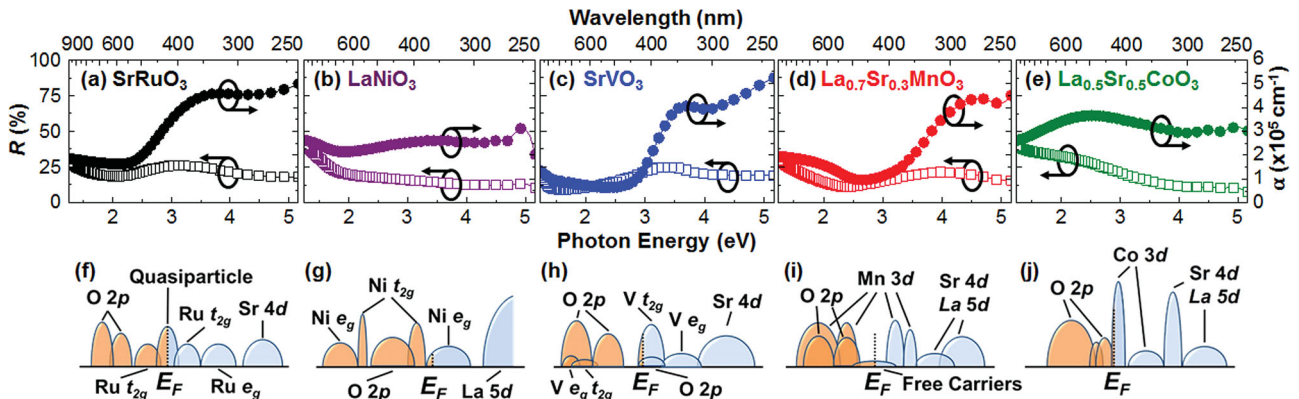


Figure 2. Reflectance (R , left ordinate) and absorption coefficient (α , right ordinate) for 50 nm thin films of (a) SrRuO₃, (b) LaNiO₃, (c) SrVO₃, (d) La_{0.7}Sr_{0.3}MnO₃, and (e) La_{0.5}Sr_{0.5}CoO₃. (f–j) Corresponding schematic band diagrams for the materials in (a–e).

In turn, these materials can be used as the foundation for a range of energy devices. We begin by probing model photovoltaic devices that provide us insight into the nature of the TiO₂/“metallic” oxide junction type and the nature of the photocurrent generation to inform the use of these materials as photocatalysts. The photovoltaic devices studied here have a generic structure of 100 nm 10% SnO₂-doped In₂O₃ (ITO)/100 nm anatase TiO₂/50 nm “metallic” oxide (Figure 3a). Dark current-voltage (I - V) studies have been completed on these heterojunctions to extract values for the TiO₂/“metallic” oxide barrier heights (see Supporting Information, Figure S3). Based on published values of work functions for these “metallic” oxide materials,^[10,37,43–51] we expect Schottky barrier heights between the TiO₂ and SrRuO₃, La_{0.7}Sr_{0.3}MnO₃, LaNiO₃, La_{0.5}Sr_{0.5}CoO₃, and SrVO₃ of 1.3 ± 0.1 eV, 1.1 ± 0.1 eV, ~ 1.0 eV, 0.7 ± 0.5 eV, and 0 eV, respectively. The error bars represent the range of work functions reported in the literature and the value for LaNiO₃ (~ 1.0 eV) is based on only

one published value. When possible, we applied standard Richardson-Nordheim equation fitting procedures to the dark I - V data to extract experimental barrier heights. For all materials, the experimentally measured barrier heights are consistent with those values noted above; however, for devices based on LaNiO₃ and La_{0.5}Sr_{0.5}CoO₃ the ideality factor from the fit was >2 and thus the accuracy of those fits are questioned. Regardless, these analyses allow us to identify three different classes of heterojunctions – n-n Schottky (based on SrRuO₃ and LaNiO₃), n-n ohmic junctions (based on SrVO₃), and p-n Schottky (based on La_{0.7}Sr_{0.3}MnO₃ and La_{0.5}Sr_{0.5}CoO₃) junctions.

Light I - V studies were completed under illumination by AM1.5G light that was filtered to remove progressively longer wavelengths (details of all light-based measurements are provided in the Supporting Information). Full light I - V data sets as a function of cut-off wavelength are provided (along with data on the light filters, Figures S4 and S5), but for simplicity we plot the short circuit current density (J_{SC}) as a function of the cut-off photon energy (Figure 3b). For all devices, except that based on SrVO₃, we observe the J_{SC} to be one-to-two orders-of-magnitude larger than the current density in the dark at zero voltage bias (J_0). We also note that despite the differences in heterojunction type, we observe the same sign of photocurrent for all TiO₂/“metallic” oxide devices and that although there are variations in the absorption coefficients of the various “metallic” oxide layers across the range of wavelengths studied, normalization of the J_{SC} by the absorbed light intensity across this same range has a negligible effect on the trends observed here.

Based on the band gap of the TiO₂, light with energy <3.4 eV (or >364 nm) is not efficiently absorbed by the TiO₂ and, in turn, the existence of J_{SC} under illumination in those conditions demonstrates that the photocurrent is generated from light absorption in the “metallic” oxide as it is the only active light

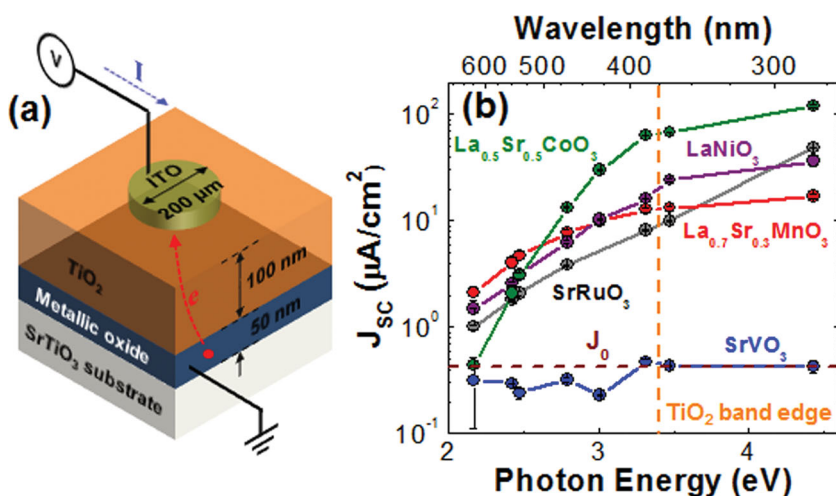


Figure 3. (a) Schematic diagram of photovoltaic device geometry consisting of 100 nm ITO/100 nm TiO₂/50 nm “metallic” oxide heterojunction devices. (b) Short-circuit current density (J_{SC}) as a function of photon energy measured under AM1.5G illumination with various longpass glass filters.

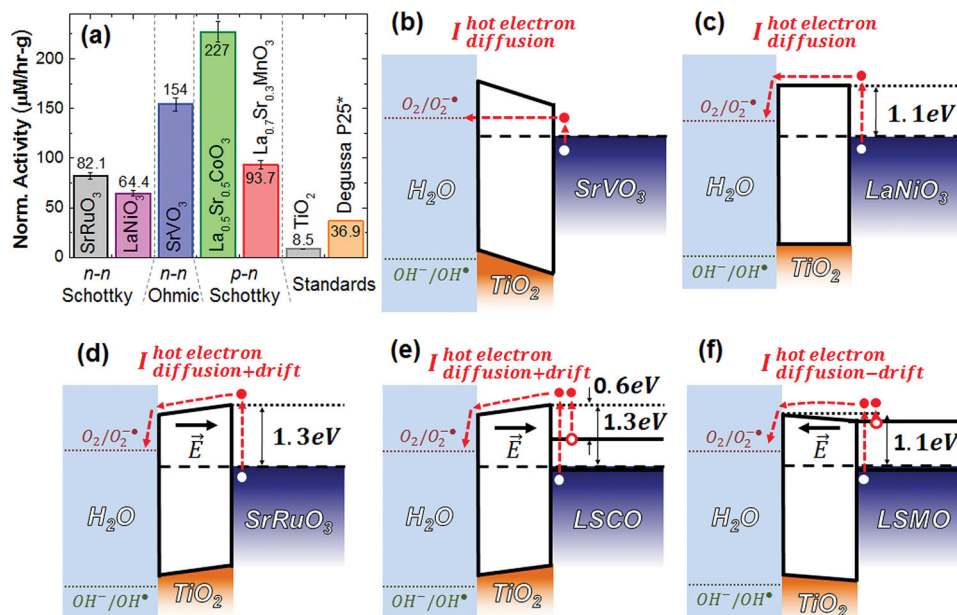


Figure 4. (a) Mass normalized methylene blue (MB) degradation activity for 10 nm TiO₂/50 nm “metallic” oxide heterojunctions devices under AM1.5G illumination (*Degussa P25 from Ref. [53]). Schematic band diagrams for the photocatalytic devices for (b) SrVO₃, (c) LaNiO₃, (d) SrRuO₃, (e) La_{0.5}Sr_{0.5}CoO₃, and (f) La_{0.7}Sr_{0.3}MnO₃. The relative reduction/oxidation potentials for pH 7 water are shown to scale on the left of each figure.

absorbing layer. Additionally, for all devices exhibiting J_{SC} above J_0 we observe (roughly) an exponential increase in the J_{SC} with increasing cutoff energy. The exponential trend is observed in both the n-n and p-n Schottky devices and suggests that as the higher energy light is filtered out, fewer of the photoexcited electrons produced in the “metallic” oxide have sufficient energy to overcome the Schottky barrier and therefore fewer of these electrons diffuse across the TiO₂/“metallic” oxide interface. We conclude, therefore, that the mechanism of photocurrent generation in these devices is likely hot electron injection. Devices exhibiting $J_{SC} \approx J_0$ (i.e., those based on SrVO₃) exhibit no photocurrent response because the ohmic junction does not provide a driving force for photocurrent flow (a more detailed description of each photovoltaic device as well as proposed device band diagrams are provided in the Supporting Information and Figure S6).

To assess the photocatalytic performance of the TiO₂/“metallic” oxide heterojunctions we measured the degradation rate of methylene blue (MB), a widely used method to evaluate and compare the visible light activities of photocatalysts.^[52,53] All photocatalytic studies were completed on 10 nm TiO₂/50 nm “metallic” oxide heterojunctions where the thickness of the TiO₂ was chosen to be sufficient to protect the “metallic” oxide from photodegradation while still being thin enough to support efficient charge transport (details of the measurements are provided in Figure S7).^[54]

The normalized MB concentration time traces for all the heterojunctions and control samples showed pseudo-first order kinetics allowing the calculation of mass-normalized photocatalytic activity (Figure 4a and Figure S8). We observe the highest mass-normalized activity for the La_{0.5}Sr_{0.5}CoO₃-based devices and the lowest for the LaNiO₃-based devices. It should also be noted that the activity in the La_{0.5}Sr_{0.5}CoO₃-

based devices is 27- and 6.2-times larger than that for a single-layer TiO₂ film and nanopowder Degussa P25 samples, respectively.^[53]

The trends in mass-normalized photocatalytic activity are not simply understood in the context of light absorption alone, but are a complex function of the interplay of the electronic structure of the “metallic” oxide, light absorption, junction type, barrier height, and built-in electric field. Additionally, to understand the performance of the devices one generally needs to consider the contributions of both drift and diffusion currents to the overall response. Previous studies of electronic transport in anatase thin films,^[55] however, have revealed that the diffusion length of electrons in anatase is on the order of only 1 nm. Thus in the case of the photovoltaic device (where there is a 100 nm thick TiO₂ layer) the diffusion current is expected to be negligible and does not contribute significantly to the short-circuit current density while in the case of the photocatalytic device (where there is only a 10 nm thick TiO₂ layer) this likely will not be the case. To further facilitate this discussion and to aid our understanding of the operation of the photocatalytic devices we present proposed schematic band diagrams (Figure 4b–f) meant to qualitatively describe the proposed processes active in each layer. Construction of these band diagrams is informed by highlighting a few similarities among the various devices. First, for all Schottky devices, the TiO₂ layer is fully depleted as a result of the 4-to-6 order-of-magnitude difference in the carrier concentration between the TiO₂ (10^{15} – 10^{17} cm⁻³) and the “metallic” oxides. Second, because the “metallic” oxides have a carrier concentration of 10^{21} – 10^{22} cm⁻³, the solution has low ionic conductivity (neutral pH, low MB concentration), and the TiO₂ is only 10 nm thick, the band alignment of the TiO₂ is likely predominantly controlled by the “metallic” oxide and not affected by the reduction/oxidation couples. In other words,

strong pinning or bending of the band structure of TiO_2 as a result of the contact with the solution is not expected.

With these similarities in mind, we now discuss the differences among the various devices: first we discuss devices having no built-in electric field in the TiO_2 (SrVO_3 and LiNiO_3), second we discuss the devices in which the built-in electric field in the TiO_2 enhances the photocatalytic activity by adding a drift current in the same direction as the diffusion current (SrRuO_3 and $\text{La}_{0.5}\text{Sr}_{0.5}\text{CoO}_3$), and lastly we discuss the case of the device which has a built-in electric field in the TiO_2 that inhibits (some) of the diffusion current by adding a drift current that opposes the diffusion current ($\text{La}_{0.7}\text{Sr}_{0.3}\text{MnO}_3$).

The SrVO_3 - and LaNiO_3 -based devices both have no built-in electric field in the TiO_2 . In the case of the SrVO_3 -based device (Figure 4b), this is because the work function of the “metallic” oxide is lower than the E_F (i.e., the separation between the Fermi state and vacuum level) of the TiO_2 which results in the formation of an ohmic junction, just as in traditional semiconductor-metal devices. Because the junction is ohmic, there is an accumulation of charges in the TiO_2 and no barrier to hot electron diffusion from the SrVO_3 into the TiO_2 . The absence of such a barrier accounts for the SrVO_3 -based device possessing the second largest measured mass-normalized photocatalytic activity ($154 \mu\text{M}/\text{hr}\cdot\text{g}$) despite having the lowest absorption of the AM1.5G spectrum (33%). For the LaNiO_3 -based device (Figure 4c), the work function of the “metallic” oxide and the E_F of TiO_2 are approximately the same magnitude, resulting in the formation of a flat-band Schottky junction with a barrier height of ~ 1.0 eV and, as a result of the lack of band bending, no built-in electric field in the TiO_2 . The Schottky barrier serves as a barrier to hot electron transport from the “metallic” oxide into the TiO_2 and the lack of any additional driving force (i.e., the lack of built-in electric field in the TiO_2) accounts for the LaNiO_3 -based devices displaying the lowest observed mass-normalized photocatalytic activity despite having the second highest absorption of the AM1.5G spectrum (50%). This analysis demonstrates that in the design of all-oxide heterojunction devices based on correlated “metallic” oxides for photocatalysis the presence of an ohmic junction can potentially enhance the photocatalytic activity by maximizing the hot electron transport via diffusion from the “metallic” oxides to the wide band gap oxide.

The SrRuO_3 - and $\text{La}_{0.5}\text{Sr}_{0.5}\text{CoO}_3$ -based devices (Figure 4d and e, respectively) both have a built-in electric field in the TiO_2 which enhances the photocatalytic activity by adding an additional driving force for the transfer of hot electrons injected into the TiO_2 from the “metallic” oxide to the solution interface. This electric field produces a drift current similar to that seen in traditionally Schottky junction devices. For both devices, the work function of the “metallic” oxide is larger than the E_F of the TiO_2 which results in the formation of a Schottky junction and barrier heights of 1.3 ± 0.1 eV and 0.6 ± 0.5 eV for the SrRuO_3 - and $\text{La}_{0.5}\text{Sr}_{0.5}\text{CoO}_3$ -based devices, respectively. It is this large difference in barrier heights along with the fact that $\text{La}_{0.5}\text{Sr}_{0.5}\text{CoO}_3$ absorbs a higher percentage of the AM1.5G spectrum (53%) than SrRuO_3 (44%) that accounts for the 2.7-times higher mass-normalized activity of the $\text{La}_{0.5}\text{Sr}_{0.5}\text{CoO}_3$ device compared to the SrRuO_3 device. It should also be noted that owing to the presence of a band gap in the $\text{La}_{0.5}\text{Sr}_{0.5}\text{CoO}_3$

which is not present in the SrRuO_3 , there exists a small population of electrons in the conduction band of the $\text{La}_{0.5}\text{Sr}_{0.5}\text{CoO}_3$ for which there is a lower barrier to injection into the TiO_2 . By combining this comparison with our previous discussion of the ohmic and Schottky flat-band devices, we surmise that the lower Schottky barrier when combined with high light absorption and a built-in electric field that enhances hot electron transport to the solution interface yields the best performing all-oxide heterojunction devices based on correlated “metallic” oxides.

Lastly we discuss the case of $\text{La}_{0.7}\text{Sr}_{0.3}\text{MnO}_3$ -based devices (Figure 4f) where there is a p-n Schottky junction with the TiO_2 and a built-in electric field in the TiO_2 that opposes the hot electron diffusion current. The work function of the $\text{La}_{0.7}\text{Sr}_{0.3}\text{MnO}_3$ is smaller in value than the E_F of TiO_2 , but, unlike the case of the SrVO_3 device in which an ohmic junction is formed, $\text{La}_{0.7}\text{Sr}_{0.3}\text{MnO}_3$ forms a Schottky junction with TiO_2 because $\text{La}_{0.7}\text{Sr}_{0.3}\text{MnO}_3$ is a p-type “metallic” oxide (i.e., the n-type TiO_2 is completely depleted of free electrons by the transfer of holes from the $\text{La}_{0.7}\text{Sr}_{0.3}\text{MnO}_3$ when the junction is formed). As in the case of $\text{La}_{0.5}\text{Sr}_{0.5}\text{CoO}_3$, we point out that the presence of a band gap results in a small population of electrons in the conduction band of the $\text{La}_{0.7}\text{Sr}_{0.3}\text{MnO}_3$ for which there is a significantly lower barrier (~ 0.1 eV) to the injection of hot electrons into the TiO_2 . The net result is that while the $\text{La}_{0.7}\text{Sr}_{0.3}\text{MnO}_3$ has the second lowest absorption, it exhibits a mass-normalized activity slightly higher than that of the SrRuO_3 , but significantly lower than the $\text{La}_{0.5}\text{Sr}_{0.5}\text{CoO}_3$ devices due to the completing effects of barrier height, electric field, and electronic structure. This analysis suggests that it is crucial to understand the direction of band bending or the built-in electric field as it plays a significant role in driving the hot electrons in the devices.

In conclusion, we have studied the optical, photovoltaic, and photocatalytic response of TiO_2 /correlated “metallic” oxide heterojunctions. Ellipsometric studies of the “metallic” oxides reveal that as a result of the complex electronic structure of these materials, they possess low reflectance and high absorption coefficients that enable up to 53% of AM1.5G light to be absorbed by only 50 nm thick films. Upon studying the photovoltaic and photocatalytic response of heterojunctions based on these materials we observe a number of important features. First, by controlling the work function and carrier type of the “metallic” oxide, we can produce three different types of heterojunctions: n-n Schottky, n-n ohmic, and p-n Schottky junctions. In turn, this gives rise to a range of different photovoltaic responses that are dominated by hot electron injection from the “metallic” oxide into the TiO_2 . Photocatalytic studies based on these materials reveal that the activity of the heterostructures is highest for Schottky junctions where the “metallic” oxide possesses strong light absorption, the device has a low barrier height, and the built-in electric field in the TiO_2 enhances hot electron transport from the “metallic” oxide to the solution interface. Additionally, heterostructures exhibiting ohmic junctions (i.e., no barrier to hot electron diffusion) can overcome limitations in light absorption to show enhanced activity. In turn, the combination of “metallic” oxide with TiO_2 enables the production of systems that greatly outperform TiO_2 films alone and other common TiO_2 -based nanoparticle systems. These conclusions provide a framework for the rational design

of photoelectrochemical all-oxide devices utilizing hot electron injection and illustrate how correlated electron systems can significantly enhance performance in energy systems.

Supporting Information

Supporting Information is available from the Wiley Online Library or from the author.

Acknowledgements

B. A. Apgar and S. Lee contributed equally to this work. The authors acknowledge support by the International Institute for Carbon-Neutral Energy Research (WPI-I2CNER), sponsored by the Japanese Ministry of Education, Culture, Sport, Science and Technology and support provided by the Strategic Research Initiatives Program of the College of Engineering at the University of Illinois at Urbana-Champaign. Experiments were carried out in part in the Materials Research Laboratory Central Facilities. The authors thank N. Bronn, N. Mason, and J. Soares for fruitful discussions related to electronic transport and light absorption studies.

Received: July 9, 2013

Revised: August 17, 2013

Published online: September 17, 2013

- [1] M. G. Walter, E. L. Warren, J. R. McKone, S. W. Boettcher, Q. Mi, E. A. Santori, N. S. Lewis, *Chem. Rev.* **2010**, *110*, 6446.
- [2] A. Fujishima, T. N. Rao, D. A. Tryk, *J. Photochem. and Photobiology C* **2000**, *1*, 1.
- [3] R. C. Kainthla, B. Zelenay, J. O'M Bockris, *J. Electrochem. Soc.* **1986**, *133*, 248.
- [4] T. A. Abshire, G. L. Richmond, *J. Phys. Chem. B* **2000**, *104*, 1602.
- [5] K. Maeda, K. Domen, *J. Phys. Chem. Lett.* **2010**, *1*, 2655.
- [6] A. Paracchino, V. Laport, K. Sivula, M. Graetzel, E. Thimsen, *Nature Mater.* **2011**, *10*, 456.
- [7] Y. J. Hwang, A. Boukai, P. Yang, *Nano Lett.* **2008**, *9*, 410.
- [8] P. D. Ye, *J. Vac. Sci. Technol. A* **2008**, *26*, 697.
- [9] H. L. Ju, C. Kwon, Q. Li, R. L. Greene, T. Venkatesan, *Appl. Phys. Lett.* **1994**, *65*, 2108.
- [10] M. A. Torija, M. Sharma, M. R. Fitzsimmons, M. Varela, C. Leighton, *J. Appl. Phys.* **2008**, *104*, 023901.
- [11] J. B. Torrance, P. Lacorre, A. I. Nazzal, E. J. Ansaldo, Ch. Niedermayer, *Phys. Rev. B* **1992**, *45*, 8209.
- [12] A. Urushibara, Y. Moritomo, T. Arima, A. Asamitsu, G. Kido, Y. Tokura, *Phys. Rev. B* **1995**, *51*, 14103.
- [13] S. Mukherjee, R. Ranganathan, P. S. Anilkumar, P. A. Joy, *Phys. Rev. B* **1996**, *54*, 9267.
- [14] G. Cao, S. McCall, M. Shepard, J. E. Crow, R. P. Guertin, *Phys. Rev. B* **1997**, *56*, 321.
- [15] P. Dougier, J. C. C. Fan, J. B. Goodenough, *J. Solid State Chem.* **1975**, *14*, 247.
- [16] L. W. Martin, Y.-H. Chu, R. Ramesh, *Mat. Sci. Eng. R* **2010**, *68*, 89.
- [17] R. L. Ritums, N. J. Wu, D. Liu, Q. Zhong, Y. M. Chen, X. Zhang, P. C. Chou, A. Ignatiev, *Proceedings Of The Tenth IEEE International Symposium On Applications Of Ferroelectrics, Applications of Ferroelectrics* **1996**, *2*, 417.
- [18] C. L. Chen, Y. Cao, Z. J. Huang, Q. D. Jiang, Z. Zhang, Y. Y. Sun, W. N. Kang, L. M. Dezaneti, W. K. Chu, C. W. Chu, *Appl. Phys. Lett.* **1997**, *71*, 1047.
- [19] K. M. Satyalakshmi, R. M. Mallya, K. V. Ramanathan, X. D. Wu, B. Brainard, D. C. Gautier, N. Y. Vasanthacharya, M. S. Hegde, *Appl. Phys. Lett.* **1993**, *62*, 1233.
- [20] M. Imada, A. Fujimori, Y. Tokura, *Rev. Mod. Phys.* **1998**, *70*, 1039.
- [21] Y. Tokura, N. Nagaosa, *Science* **2000**, *288*, 462.
- [22] E. Dagotto, Y. Tokura, *MRS Bull.* **2008**, *33*, 1037.
- [23] A. Moreo, S. Yunoki, E. Dagotto, *Science* **1999**, *283*, 2034.
- [24] E. Dagotto, T. Hotta, A. Moreo, *Phys. Rep.* **2001**, *344*, 1.
- [25] M. B. Salamon, M. Jaime, *Rev. Mod. Phys.* **2001**, *73*, 583.
- [26] G. Koster, L. Klien, G. Rijnders, J. S. Dodge, C.-B. Eom, D. H. A. Blank, M. R. Beasley, *Rev. Mod. Phys.* **2012**, *84*, 253.
- [27] K. Fujioka, J. Okamoto, T. Mizokawa, A. Fujimori, I. Hase, M. Abbate, H. J. Lin, C. T. Chen, Y. Takeda, M. Takano, *Phys. Rev. B* **1997**, *56*, 6380.
- [28] T. Saitoh, T. Mizokawa, A. Fujimori, M. Abbate, Y. Takeda, M. Takano, *Phys. Rev. B* **1997**, *56*, 1290.
- [29] X. Gray, A. Janotti, J. Son, J. M. LeBeau, S. Ueda, Y. Yamashita, K. Kobayashi, A. M. Kaiser, R. Sutarto, H. Wadati, G. A. Sawatzky, C. G. Van de Walle, S. Stemmer, C. S. Fadley, *Phys. Rev. B* **2011**, *84*, 075104.
- [30] C. Ma, Z. Yang, S. Picozzi, *J. Phys.: Condens. Matter.* **2006**, *18*, 7717.
- [31] M. Karolak, T. O. Wehling, F. Lechermann, A. I. Lichtenstein, *J. Phys.: Condens. Matter.* **2011**, *23*, 085601.
- [32] E. D. Palik, *Handbook of Optical Constants of Solids*, Academic Press, Boston, MA, USA **1985**.
- [33] K.-H. Goetz, D. Bimberg, H. Jurgensen, J. Selders, A. V. Solomonov, G. F. Glinskii, M. Razeghi, *J. Appl. Phys.* **1993**, *54*, 4543.
- [34] J. Micallef, B. L. Weiss, *Opt. Quant. Electron.* **1991**, *23*, 669.
- [35] G. E. Jellison, L. A. Boatner, J. D. Budai, B.-S. Jeong, D. P. Norton, *J. Appl. Phys.* **2003**, *93*, 9537.
- [36] J. S. Lee, Y. S. Lee, T. W. Noh, K. Char, J. Park, S.-J. Oh, J.-H. Park, C. B. Eom, T. Takeda, R. Kanno, *Phys. Rev. B* **2001**, *64*, 245107.
- [37] S. Lee, B. A. Apgar, L. W. Martin, *Adv. Energy Mater.* DOI: 10.1002/aenm.201201116.
- [38] M. K. Stewart, C.-H. Yee, J. Liu, M. Kareev, R. K. Smith, B. C. Chapler, M. Varela, P. J. Ryan, K. Haule, J. Chakhalian, D. N. Basov, *Phys. Rev. B* **2011**, *83*, 075125.
- [39] L. V. Nomerovannaya, A. A. Makhnev, A. Yu. Romyantsev, *Phys. Solid State* **1999**, *41*, 1322.
- [40] A. Kowalczyk, A. Slebarski, A. Szajek, J. Baszynski, A. Winiarski, *J. Magn. Magn. Mater.* **2000**, *212*, 107.
- [41] P. Ravindran, P. A. Korzhavyi, H. Fjellvag, A. Kjekshus, *Phys. Rev. B* **1999**, *60*, 16423.
- [42] T. Saitoh, T. Mizokawa, A. Fujimori, M. Abbate, Y. Takeda, M. Takano, *Phys. Rev. B* **1997**, *56*, 1290.
- [43] J. Hartmann, M. Neilson, R. N. Lamb, K. Watanabe, J. F. Scott, *Appl. Phys. A* **2000**, *70*, 239.
- [44] X. Fang, T. Kobayashi, *Appl. Phys. A Suppl.* **1999**, *69*, S587.
- [45] J. F. Scott, *Jpn. J. Appl. Phys.* **1999**, *38*, 2272.
- [46] G. Xiong, R. Shao, T. C. Droubay, A. G. Joly, K. M. Beck, S. A. Chambers, W. P. Hess, *Adv. Funct. Mater.* **2007**, *17*, 2133.
- [47] S. Aizaki, T. Yoshida, K. Yoshimatsu, M. Takizawa, M. Minohara, S. Ideta, A. Fujimori, K. Gupta, P. Mahadevan, K. Horiba, H. Kumigashira, M. Oshima, *Phys. Rev. Lett.* **2012**, *109*, 056401.
- [48] M. Minohara, R. Yasuhara, H. Kumigashira, M. Oshima, *Phys. Rev. B* **2010**, *81*, 235322.
- [49] T. Kudo, M. Tachiki, T. Kashiwai, T. Kobayashi, *Jpn. J. Appl. Phys.* **1998**, *37*, L999.
- [50] B. Nagaraj, S. Aggarwal, R. Ramesh, *J. Appl. Phys.* **2001**, *90*, 375.
- [51] A. Sawa, A. Yamamoto, H. Yamada, T. Fujii, M. Kawasaki, J. Matsuno, Y. Tokura, *Appl. Phys. Lett.* **2007**, *90*, 252102.
- [52] R. W. Matthews, *Water Res.* **1991**, *25*, 1169.
- [53] J. L. Gole, J. D. Stout, C. Burda, Y. Lou, X. Chen, *J. Phys. Chem. B* **2004**, *108*, 1230.
- [54] M. Quintana, T. Edvinsson, A. Hagfeldt, G. Boschloo, *J. Phys. Chem. C* **2007**, *111*, 1035.
- [55] H. Tang, K. Prasad, R. Sanjines, P. E. Schmid, F. Levy, *J. Appl. Phys.* **1994**, *75*, 2042.